CERN/SPSC/90-22
SPSC/P253
20 July 1990

PROPOSAL FOR
A PRECISION MEASUREMENT OF ε'/ε IN CP VIOLATING $K^0 \to 2\pi$ DECAYS

G.D. Barr, P. Buchholz, R. Carosi, D. Coward, D. Cundy, N. Doble, L. Gatignon,
P. Grafström, G. Kesseler, H.N. Nelson and H. Wahl
CERN, Geneva, Switzerland

K.J. Peach
Physics Department, University of Edinburgh, UK

H. Blümer, K. Kleinknecht, P. Mayer, B. Renk, H. Rohrer and A. Wagner
Institut fur Physik, Universität Mainz, Germany

M. Calvetti, P. Cenci, P. Lariccia, P. Lubrano and F. Tondini
Dipartmento di Fisica, University degli Studi di Perugia, Perugia, Italy

L. Bertanza, A. Bigi, P. Calafiura, R. Casali, M.C. Carrozza, C. Cerri, R. Fantechi, I. Mannelli,*
V. Marzulli, A. Nappi, G.M. Pierazzini and F. Sergiampietri
Dipartimento di Fisica e Sezione INFN, Piss, Italy
* SCUOLA NORMALE SUPERIORE, PISA, ITALY

J. Cheze, M. De Beer, B. Peyaud, B. Vallage and J. Zsembery
DPhPE, CEN-Saclay, Gif-sur-Yvette, France

M. Holder, A. Kreutz, M. Rest, W. Weihs and R. Werthenbach
Fachbereich Physik, Universität Siegen, Germany

C. Biino, R. Cester, F. Marchetto, S. Palestini and N. Pastrone
Dipartimento di Fisica e Sezione INFN, ToMo, Italy

E. Griesmayr, M. Markytan, G. Neuhofer, M. Pemicka, F. Szonsco, A. Taurok and C.E. Wulz
Institut für Hochenergiephysik, Österreichische Akademie der Wissenschaften, Vienna, Austria

Since the discovery of CP violation in 1964 by J. Cronin and co-workers[1], substantial experimental and theoretical activity has been devoted to understanding its origin. Despite this effort, 25 years later the observation of CP violating effects is still confined entirely to the neutral kaon system. the well established decay of the long-lived neutral kaon into a pair of either charged or neutral pions at the level of $\sim 10^{-3}$ in branching ratio, and a charge asymmetry in semi-leptonic decays. The relative decay amplitudes of CP violating to CP conserving decays of the neutral kaon into pion pairs, and the magnitude of the semi-leptonic charge asymmetry δ_l are closely related by a single complex parameter ε describing the mixing of CP odd and CP even states in short- and long-lived neutral kaons:

$$K_S = \frac{1}{\sqrt{2}}\left[(K'' + \bar{K}^0) + \varepsilon(K^0 - \bar{K}^0)\right]$$

$$K_L = \frac{1}{\sqrt{2}}\left[(K^0 - \bar{K}^0) + \varepsilon(K^0 + \bar{K}^0)\right]$$

The phase of E is related by unitarity to the masses and life-times of the two physical kaon states K_S and K_L as[2]: arg & = tan-l $2(m_L - m_S) / \Gamma_S$. The charge asymmetry is

$$\delta_1 = \frac{\left(K_L \to \pi^+ l^- \nu\right) - \left(K_L \to \pi^- l^+ \nu\right)}{\left(K_L \to \pi^+ l^- \nu\right) + \left(K_L \to \pi^- l^+ \nu\right)} = 2\,\mathrm{Re}\,\varepsilon.$$

If state mixing is the only source of CP violation (Superweak model[3]), then the two ratios of decay amplitudes η_{00} and η_{+-} are both equal to the mixing parameter ε:

$$\eta_{+-} = \eta_{00} = \frac{\langle 2\pi | T | K_L \rangle}{\langle 2\pi | T | K_S \rangle} = \varepsilon \quad \text{“}$$

In the Standard Model of electroweak interactions, CP violation is accommodated naturally by the mixing of weakly interacting quark doublets following Kobayashi-Maskawa[4], where all CP violating effects are of order $\sin\theta_1 \sin\theta_2 \sin\theta_3 \sin\delta$ in the mixing angles θ_1, θ_2 and θ_3, and the phase angle δ.

In addition to CP violating effects generated by state mixing, CP violating decays may be induced through virtual transitions involving heavy quarks. The relative magnitude ε' of such transitions involving CP violation in $K^0 \to 2\pi$ decays can be conveniently defined to be:

---

1 J.H. Christenson et al., Evidence for the 2π decay of the K_2^0 meson, Phys. Rev. Lett. 13 (1964) 138.

2 T. T. Wu and C. N. Yang, Phenomenological analysis of violation of CP invariance in decay of K° and $\bar{K}^0$, Phys. Rev. Lett. 13 (1964) 380.

3 L. Wolfenstein, Violation of CP invariance and the possibility of very weak interactions, Phys. Rev. Lett. 13 (1964) 562.

4 M. Kobayashi and K. Maskawa, CP violation in the renormalizable theory of weak interaction, Progr. Theor. Physics 49 (1973) 652.

$$\varepsilon' = i / \sqrt{2}\ \mathrm{Im}\,(A_2 / A_0)\, e^{i(\delta_2 - \delta_0)}$$

in terms of the kaon decay amplitudes into isospin zero and two two-pion final states, A_0 and A_2, and the corresponding s-wave π–π scattering phase shifts δ_0 and δ_2. Allowing for direct CP violation, the equality of η_{00} and η_{+-} is then broken, and

$$\eta_{00} = \varepsilon - 2\varepsilon'$$
$$\eta_{+-} = \varepsilon + \varepsilon'.$$

The first evidence for direct CP violation has been reported by the NA31 collaboration with a value of Re $\varepsilon'/\varepsilon = (3.3 \pm 1.1) \times 10^{-3}$. Recently, the E731 experiment at Fermilab[6] has reported a value of Re ε'/ε = (-0.5* 1.5)x 10^{-3}, which neither confirms, nor contradicts the earlier CERN result. The present best estimate of ε'/ε might be the (weighted) average of these two published measurements: Re &'/G= (2.1 ± 0.9) x 10^{-3}.

Both experiments are based on a comparison of K_S and K_L decay rates into $2\pi^0$ and $\pi^+\pi^-$, where the experimental double ratios of decay rates

$$R = \frac{K_L \to 2\pi^0}{K_S \to 2\pi^0} \Big/ \frac{K_L \to \pi^+ \pi^-}{K_S \to \pi^+ \pi^-} \approx 1\text{-}6\ \mathrm{Re}\ \varepsilon'/\varepsilon$$

are 0.980 ± 0.004 (stat.) ± 0.005 (syst.) in the former[5], and 1.002 ± 0.008 (stat.) ± 0.004 (syst.) in the latter[6]. For the NA31 experiment, the statistical precision is limited by the number of $K_L + 2\pi^0$ (109 000) decays, whereas for the E731 experiment the number of events in both KL + $2\pi^0$ (49 600) andKL+Z+r(43200) contribute about equally to the statistical error.

In the near future, prospects for improvements on the experimental side areas follows: the NA31 experiment at CERN has been improved to reduce dominant systematic uncertainties and has taken new data with nearly 300000 $K_L + 2\pi^0$ decays, and correspondingly more of the other K^0 decay modes. A new result with uncertainties reduced by 30–40% can therefore be expected. The E731 experiment has about four times more statistics on tape which are still being analyzed[8]. An accuracy on Re ε'/ε in the range of 0.7 to 0.9 x 10^{-3} cart therefore be expected for each of the two experiments. The PS 195 experiment at LEAR[9] gives an independent measurement but will not be competitive at this level of accuracy[10].

---

5 H. Burkhardt et al., First evidence for direct CP violation, Phys. Lett. B206 (1988) 169.
6 J. R. Patterson et al., Determination of Re ε'/ε by the simultaneous detection of the four $K_{S,L} \to \pi\pi$ decay modes, Phys. Rev. Lett. 64 (1990) 1491.
7 NA31 Collaboration, Memorandum CERN/SPSC/87-48, SPSC/P174/Add. 4 (1987).
8 H. Yamamoto, A recent result on CP violation by E731 at Fermilab, Proc. SLAC Summer Institute (1989) and EFI 90-13.
9 L. Adiels et al., Tests of CP violation with K^0 and $\bar{K}^0$ at LEAR, Proposal CERN/PSCC/85-6 (1985).
10 P. Pavlopoulos, First results from the CPLEAR experiment, EP Seminar, CERN, 6 June 1990.

On the theoretical front, some progress has been achieved in recent years on estimating &'/&in the Standard Model. There are several sources of uncertainty in these calculations, including the mass of the top quark. In particular, once the top quark becomes heavier than the W and Z, additional diagrams contribute [1] which reduce the magnitude of&'/&. A recent review[12] gives &'/&= $(1\pm0.5)\times10^{-3}$ for $m_t \approx 100$ GeV, reducing to near zero or even negative for m_t larger than about 200 GeV.

It is the aim of the proposed experiment to measure Reε'/ε with an accuracy of 2×10^{-4}.

1. PRINCIPLE OF THE EXPERIMENT

The measurement of &'/&is obtained by a comparison of the relative decay rates of short- and long-lived neutral kaons into two neutral and two charged pions:

$$\mathrm{Re}\,\varepsilon'/\varepsilon = \frac{1}{6}\left\{1 - \left|\eta_{00}/\eta_{+-}\right|^2\right\} = \frac{1}{6}\left\{1 - \frac{K_L \to 2\pi^0}{K_S \to 2\pi^0} \div \frac{K_L \to \pi^+\pi^-}{K_S \to \pi^+\pi^-}\right\}.$$

It is obvious but important that in this comparison the detection efficiencies cancel in principle if the result is evaluated independently for different kaon momenta and decay positions, and if K_S and K_L beams coincide in space at the position of the detector. In order to achieve this, a nearly collinear K_S and KL beam scheme is proposed, where K_S and K_L are produced concurrently and distinguished by tagging of the protons producing the K_S component. In this way differences and variations in detection efficiencies for K_S and KL decays become unimportant, as do rate dependent effects introduced by accidental activity in the detector elements.

According to previous experience, the dominant error sources are, in order of importance:

i) $K_L + 2\pi^0$ event statistics;
ii) possible differences in $2\pi^0$ and $\pi^+\pi^-$ reconstructed kaon energy scales;
iii) background to $K_L \to 2\pi^0$ by K_L –> $3\pi^0$ decays with only four detected photons;
iv) background to $K_L + \pi^+\pi^-$ decays from residual three-body decays, especially $K_L + \pi e\nu$ and $K_L \to \pi^+\pi^-\pi^0$;
v) differential effects of accidental activity in the detector between K_S and K_L.

---

11 J.M. Flynn and L. Randall, The electromagnetic penguin contribution to ε'/ε for large top quark mass, Phys. Lett. 224B (1989) 221.

12 G. Buchalla, A.J. Buras and M.K. Harlander. The anatomy of ε'/ε in the Standard Model, Preprint MPI-PAE/Pth 63/89 and TUM-T31-3/89 (1989).

The number of events required is by far the most important experimental problem. Each of the other effects have contributed 0.2 to 0.3×10^{-3} uncertainty to ε'/ε. Systematic effects due to a difference in energy scales can be reduced by a suitable choice of K^0 production spectra and appropriate analysis, at the expense of the statistical error (see below). Uncertainties due to background subtractions are decreased by reducing background levels both for $K_L + 2\pi^0$ and $K_L \rightarrow \pi^+\pi^-$ decays. Accidental effects are reduced substantially if all four decay modes are observed concurrently. These concepts form the basic idea of the present proposal.

The proposed experiment is designed to handle a tenfold increase in beam intensity and event rates as compared to NA31. A magnet spectrometer is planned to reduce background in the charged pion mode, and a fast liquid xenon photon detector for neutral pion decays with resolution superior to the existing liquid argon/lead sandwich calorimeter to reduce the backgrounds in the neutral mode.

2. THE K^0 BEAM

The basic advantages of the scheme adopted by experiment NA31 remain in comparing the $\pi^0\pi^0$ and $\pi^+\pi^-$ decay rates from distinct K_L and K_S beams which enter a common decay region along a path entirely contained in vacuum[13]. The principal improvement that can be brought to bear on possible sources of systematic error, such as accidentals and time variations in the detector, is to record the two decay modes from both K_L and K_S beams at the same time and from the same fiducial length. Possible differences in the response of the detector to the two alternate beams are thereby eliminated.

Some consideration has also been given to developments of the proposed beam design, adapted to an extensive programme of kaon physics, which might include:

i) the use of the K_L beam alone at increased intensity to search for rare decays (e.g. $K_L + \pi^0 e^+ e^-$) at sensitivities in branching ratio $\sim 10^{-11}$;

ii) the substitution of the front end of the beam by an achromatic charged-particle transport system, providing simultaneous, collinear beams of K^+ and K^- to allow an accurate comparison of the $\pi^\pm\pi^+\pi^-$ decay dynamics at the 10-3 level, also depending on the value of ε'/ε (see Appendix).

---

13 H. Burkhardt et al., The beam and detector for a high-precision measurement of CP violation in neutral kaon -- decay, Nucl. Instrum. Methods, A268 (1988) 116.

2.1 COMBINED K_L AND K_S BEAMS

It is important, in order to eliminate all sources of systematic differences in the detection of K_L and K_S decays, to arrange the two beams to be nearly collinear"], i.e. converging at an angle comparable to the beam divergence.

The proposed layout is shown schematically in Fig. 1. A primary proton beam (at an intensity of $\sim 10^{12}$ ppp) is used to produce the K_L beam at a small angle (2.4 mrad). After a first acceptance-limiting collimator, the remaining protons (and other charged particles) emerging from the target are deviated away from the K_L line by a sweeping magnet. A bent, single crystal is appropriately arranged to channel and deviate a small fraction of the primary protons[14,15] (-3 x 10^7 ppp) back towards the K_L line**), whilst all other charged particles are absorbed in a beam dump/collimator assembly***). The resulting beam of protons thus defined passes through a frost tagging counter and is then magnetically deflected onto the KL line, along which it is transported and refocused. It is finally deflected again so as to pass through a second tagging counter and strike the K_S target, which is located 72 mm above the K_L beam axis at the chosen production angle (4.2 mrad). From this target the K_S beam is defined by collimation over a length of 6 m so as to converge towards the detector at an angle of 0.6 mrad to the K_L beam. The exit of the K_S collimator nearly coincides longitudinally with the end of the last of a series of three collimators, which are designed to define and clean the K_L beam so that background from the defining collimator cannot reach the detector outside the central beam passage. Thus K_L and K_S decays are observed simultaneously from the closely adjacent fiducial regions of the two beams emerging from their respective collimators over an effective length ($\sim 2\tau_S$), where there are enough K_S to match the numbers of $K_L \to \pi\pi$ (see Section 2.2 below). In this scheme, the K_S beam is not moved, but is located in the optimum longitudinal position with respect to the detector acceptance (Sections 4 and 5).

---

*) A finite separation of the Ks target with respect to the KL beam lie is required to permit different collimator apertures (radius 2.4 *mm* and 28 mm *respectively)* for the two beams, with a minimum of shielding between them. Moreover, it is important to place the production target and a lead converter followed by an anticounter (to define the start of the decay region for Ks) outside the high neutron and photon fluxes contained in the K_L beam.

14 F. Bak et al., Detailed investigation of the channeling phenomena involved in bending of high-energy beams by means of crystals, Nucl. Phys. B242 (1984) 1.

15 S.1. Baker et al., First operation with a crystal septum to replace a magnet in a charged particle beam, Nucl. Instrum. Methods A234 (1985) 602.

**) This technique has been tested successfully by members of SL/EA and NA43 (Aarhus, Strasbourg) groups using the H8 high-resolution proton beam. A fraction as high as several percent of the 450 GeV/c protons were observed to have been deflected through a bending angle of 7.4 mrad by a 50 mm long silicon crystal.

***) The bent crystal uniquely combines three features of interest to the present application

i) attenuation of the proton intensity by a variable factor -10%

ii) selection of a small emittance beam, suitable for transport to the Ks target;

iii) deflection of this beam in a direction opposite to that of the preceding magnet without canceling its sweeping action on other charged particles ($\pi^{\pm}, \mu^{\pm}$).

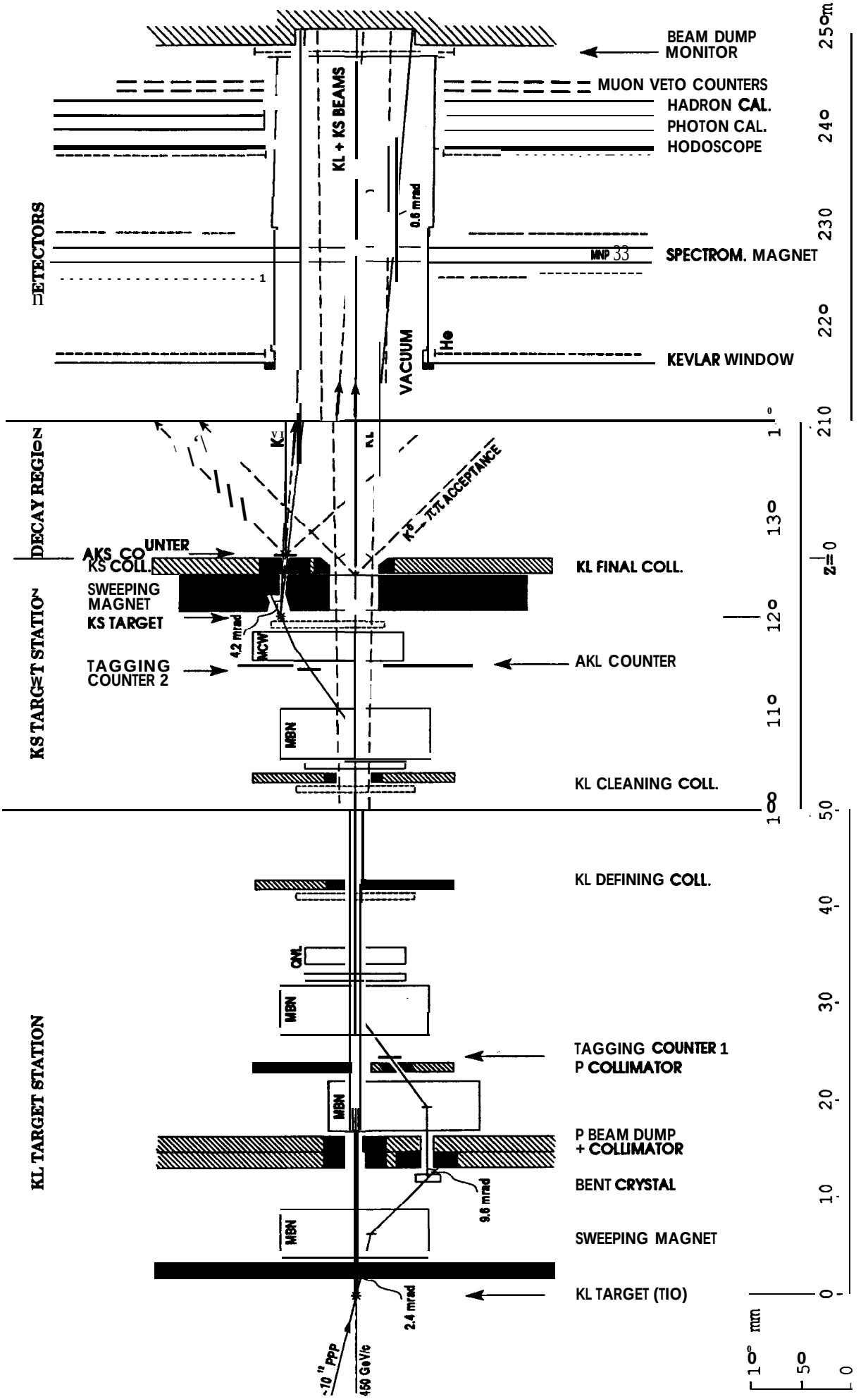

Fig. 1 Schematic layout of combined K_L and K_S beams (vertical section)

The decay fiducial region, shown schematically in Fig. 2, is contained at the upstream end of a 330 m^3 cylindrical vacuum tank of inside diameter 1.9 m over the first 40 m and 2.4 m over the remaining 48 m of its length. This is constructed of sections of the tank used in the NA31 experiment and should be evacuated to a pressure $<10^{-3}$ mbar. It is terminated by a thin window similar to the NA31 Kevlar window, but (if possible) of thickness reduced to ~0.8 mm. The centre of the window is traversed by a beam pipe of inside diameter ranging from 148 to 160 mm, which allows the two convergent beams to be transported in vacuum through holes in the various elements of the detector until they reach a profile and intensity monitor and finally enter a beam dump situated-250 m from the K_L target.

The origin of the decays in the K_L or the K_S beam is determined by tagging the protons transported to the K_S target. We argue that this can be done at rates up to -10^7 S-l without introducing bias between $\pi^0\pi^0$ and $\pi^+\pi^-$ decay modes. This is discussed in Section 3. Since the two beams are slightly separated in the decay region, the attribution can be checked by reconstructing the position of the vertex of charged tracks for the $\pi^+\pi^-$ decays and for the Dalitz pairs which accompany a small fraction of $\pi^0\pi^0$ decays.

Proposed parameters and counting rates for such a scheme of simultaneous, nearly-collinear K_S and K_L beams are given in Table 1.

2.2 MOMENTUM SPECTRA AND DECAY DISTRIBUTIONS

The acceptances for detection of $K^0 \rightarrow \pi^0\pi^0$ and $\pi^+\pi^-$ decays are (different) functions of their momentum p and longitudinal position z. Therefore, the momentum spectra of accepted K_L and K_S decays should be adjusted to be similar by:

i) keeping the length from the K_S target to collimator relatively short (e.g. 6 m, close to one K_S lifetime, which can be shown to maximize the K_S flux with respect to collimator-produced background);

ii) choosing an appropriate production angle for K_S given the K_L production angle, e.g. 4.2 rnrad and 2.4 rnrad, respectively, Figs. 3 and 4.

However, the vertex (z) distributions of K_L and K_S decays are naturally very different and a method to compensate for this in the analysis is suggested.

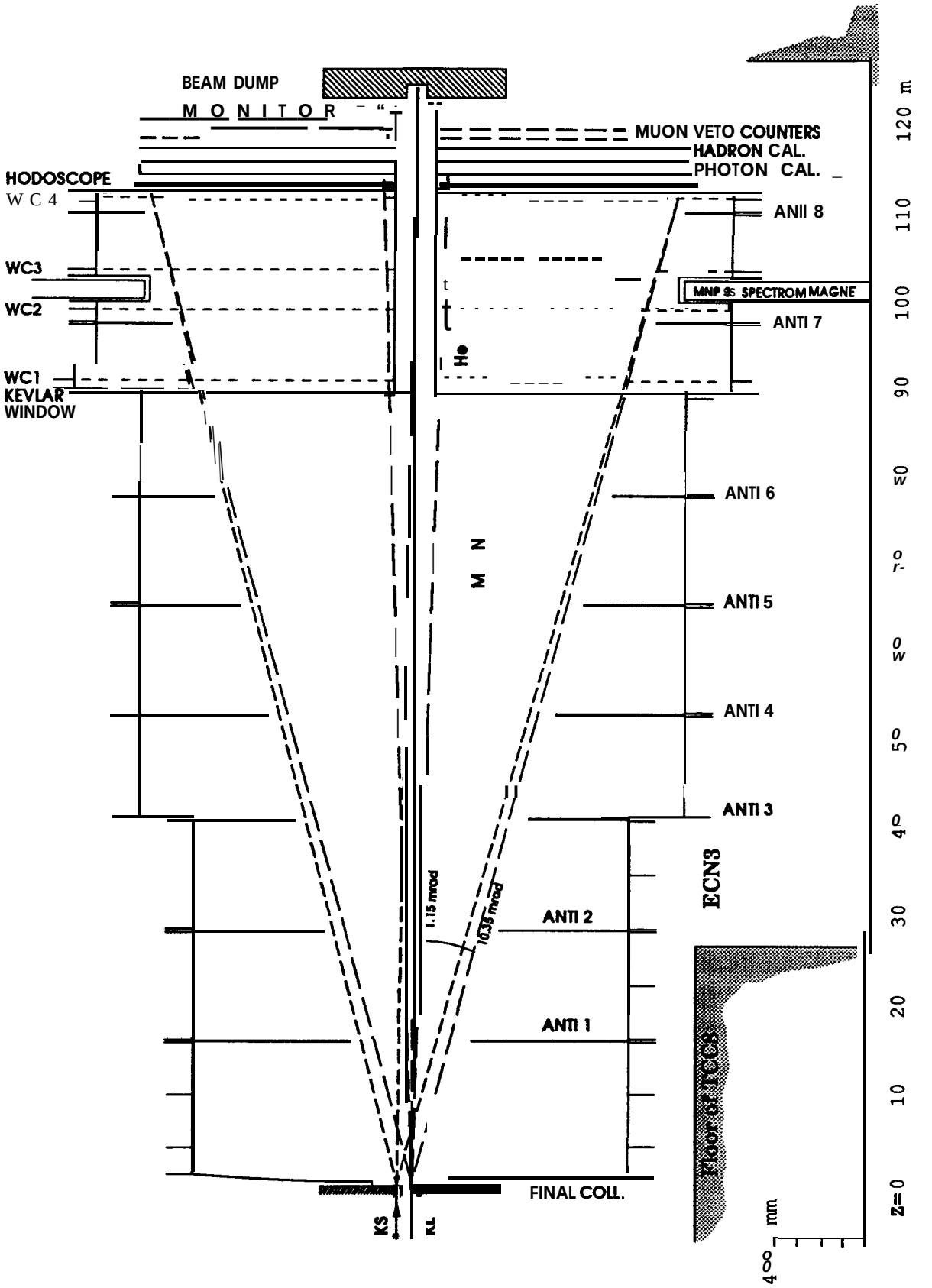

Fig. 2 Schematic layout of vacuum tank and spectrometer with arrangement of anticounter "pockets" (vertical section)

TABLE 1 Characteristics of proposed combined K^o beam

	Simultaneous, nearly-collinear beams of K_L + K_S	
Protons per pulse on target:	1.5 " 10^{12}	3 " 10^7
Spill -2.5 s, Cycle time 14.4s		
Momentum p_0 (GeV/c)	450	450
Production angle (mrad)	2.4	4.2
Length of beam:		
target to last collimator (m)	126.0	6.0
last coil. to photon calorimeter (m)	114.0	
Angle of convergence to K_L beam mrad)	---	0.6
Angular acceptance of K^0 beam (mrad)	±0.15	±0.45
Radius of beam at detector (mm)	36 ± 5	54 ± 20
Radius of beam passage (mm)	74 – 80	
K^0 momentum range accepted, p(GeV/c)	70<p<170	
Fiducial length for decays (m)	$2\tau_S \approx 12$	
at mean momentum $\bar{p}$ (GeV/c)	-110	
Total K^0 per pulse at exit last coll.	~2 • 10^7	-3 " 10^2
K^0 per pulse of accepted P	6.4 •10^6	2.2 " 10^2
and decaying in fiducial length	2.2 •10^4	1.9 " 10^2
to –> $\pi^0\pi^0$	20	60
Detector acceptance for decays	0.2	
Useful decays per pulse : K^o –> $\pi^0\pi^0$	4	12
" " per hour "	1.0 " 10^3	3.0 " 10^3
" " per year "	1.5 •10^6	4.5 • 10^6
(120 days with eff. 0.5)		
Counting Rates:		
Incident protons on target (s^{-1})	6 • 10^{11}	1.2 •10^7 tagged
K^0 decays into detector (s^{-1})	~3 • 10^5	-2 " 10^2
n's through detector (s^{-1})	~2 • 10^5	-'1 " 10^4
Total rate in detector (s^{-1}) extrapolated from 1988-89 rates)	~1 • 10^6	-2 • 10^5

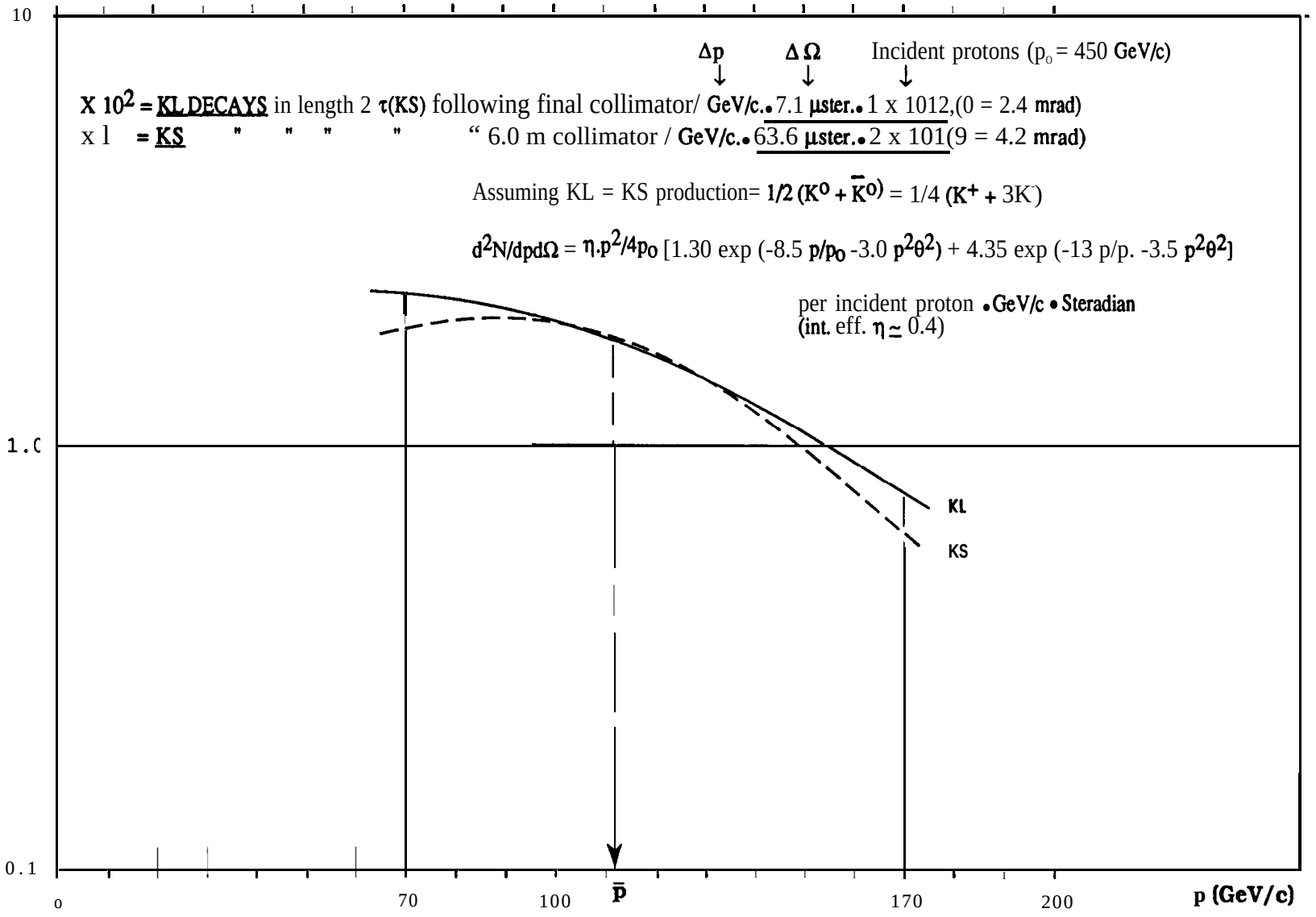

Fig. 3 K_L and K_S decay spectra

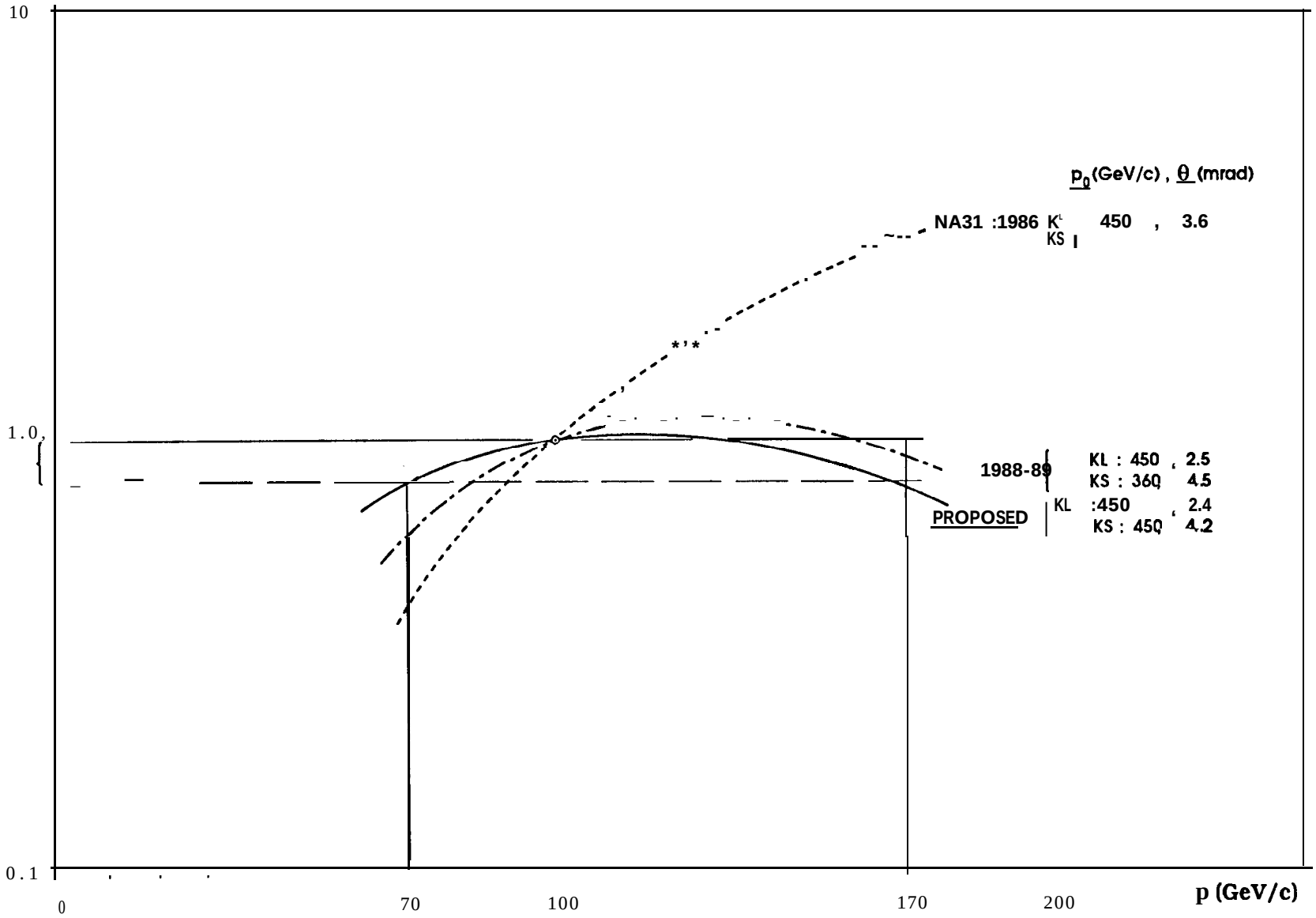

Fig. 4 K_S/K_L decay ratio, normalized to p = 100 GeV

At each K^0 momentum the measured z-scales for $\pi^0\pi^0$ and $\pi^+\pi^-$ decays are adjusted to the K_S -- anticounter (AKS) position, which is used to define sharply the upstream end of the K_S fiducial region. The upstream end of the adjacent K_L decay region is then defined to be at the same (measured) longitudinal position z. The downstream ends of the $\pi^0\pi^0$ and $\pi^+\pi^-$ decay regions are similarly defined by the measured z, and so the same for K_S and K_L, at such a distance that the number of K_S decays (and hence the statistical weight) is anyway dwindling ($> 2\tau_S$).

Over the intervening fiducial region thus defined, each K_L decay can be weighted according to the measured z position by a factor $e^{-z/\lambda(p)}$ with $\lambda(p) = (p/m) \cdot c\tau_S/(1 - \tau_S/\tau_L)$, where m is the K^0 mass and τ_S, τ_L are the K_S, K_L lifetimes, respectively. The z-distributions of K_S and (weighted) K_L decays are thereby made similar, such that corrections a(p,z) for the z-variation of acceptance (which are different for $\pi^0\pi^0$ and $\pi^+\pi^-$) cancel between K_S and K_L.

The double ratio R(p) can then be formed from the sums of numbers of events N(p,z) in a given bin of K^0 momentum p:

$$R(p) = \frac{\sum_{z_1(00)}^{z_2(00)} N(p,z)_{KL \to 00} \cdot a_{00}(p,z) \cdot e^{-z/\lambda(p)}}{\sum_{z_1(00)}^{z_2(00)} N(p,z)_{KS \to 00} \bullet a@,z)} \times \frac{\sum_{z_1(+-)}^{z_2(+-)} N(p,z)_{KS \to +-} \cdot a_{+-}(p,z)}{\sum_{z_1(+-)}^{z_2(+-)} N(p,z)_{KL \to +-} \bullet a+@,z) \; `e^{-m(p)}}$$

The overall double ratio R used to determine ε'/ε is finally obtained as the mean of R(p), taken over all bins in the range of p for which the K_L and K_S decay spectra are sufficiently similar, e.g. 70 c p < 170 GeV/c.

The introduction of the weighting factors $e^{-z/\lambda(p)}$ makes use of information, based on knowledge of the K_S (and KL) lifetimes, in addition to the measured quantities p and z. We tested the effectiveness of this weighting procedure in the presence of resolution effects (Gaussian smearing as well as tails), energy scale errors and nonlinearities by Monte Carlo. Even for uncertainties in the acceptance as large as 1 percent per metre, the bias on the double ratio can be kept below the per mine level. The weighting procedure does not deteriorate the sensitivity to the neutral energy scale. This sensitivity will be smaller than in the NA31 experiment. Also the double ratio does not depend significantly on the input value of the K_S lifetime. Moreover, it can be shown that the increase in statistical error due to the weighting is small, namely -15% for $z_2 - z_1 = 2\tau_S$.

An advantage, obtained naturally by this method, is that the fiducial length for K_L decays is defined in units of lifetimes $\lambda(p)$ and hence proportional to p, removing the l/p term with which

the production spectrum would have to be multiplied to obtain the spectrum of decays in a fixed z interval. Hence, the accepted K_L decay spectrum is rendered less steep and "harder" and a smaller production angle can be adopted for the K_S to match. The result is an improved K_S yield per incident proton and K_L and K_S decay spectra which can be made similar to within $\sim\pm 10\%$ over the range $70 < p_c < 170$ GeV/c, as demonstrated in Figs. 3 and 4.

2.3 LOCATION AND COMPATIBILITY

The beam described above (Section 2.1) is derived from primary protons of intensity $\sim 10^{12}$ per pulse. The resulting hadron and muon fluxes are such that it is practically impossible to shield neighboring experiments and the site perimeter sufficiently in an open experimental area, whilst providing maximum absorption and magnetic sweeping in the direction of the detector. We are therefore led to consider a dedicated, underground area of dimensions sufficient to house the neutral beam and experiment. The only such area at the SPS is that provided by the North Area High Intensity Facility[16], shown in Fig. 5, where an enlarged target and beam tunnel, of length 170 m, is followed by an experimental cave, 100 m long, 16 m wide and 8 m in height up to the crane.

At present two beam lines are installed in this area: one used as a primary proton and heavy ion beam transport to experiment NA38; the other is the disused beam which served the photo-production experiment NA14. These two lines are designed to receive protons alternately, so that only one of the two experiments can run at a given time.

For the combined $K_L + K_S$ beams, which are derived from a single proton beam branch, the latter NA14 line appears suitable (beam "K12", Fig. 5). The target station would be displaced upstream by some 75 m from its present position and adapted to serve as the source of the K_L beam.

However, the new K^0 beam, and notably the charged-pion spectrometer (see Fig. 2 and Section 5), would have to extend alongside NA38. This would prevent the sideways retraction of the large wire chambers of that experiment, which is the present way of gaining access to them. It is proposed, instead, to modify the support structure of these chambers to allow them to be separated in the longitudinal direction, along with the air-core magnet which is already mounted on longitudinal rails, to permit access in between them. This operation has to be carefully planned together with NA38 and executed at the appropriate time, following the current 1990-91

16 G. Brianti and N. Doble, The SPS North Area High Intensity Facility NAHIF - A review of the project and possible beams, CERN/SPS/EA 77-2, CERN/SPS/77-72/T-18 (1977).

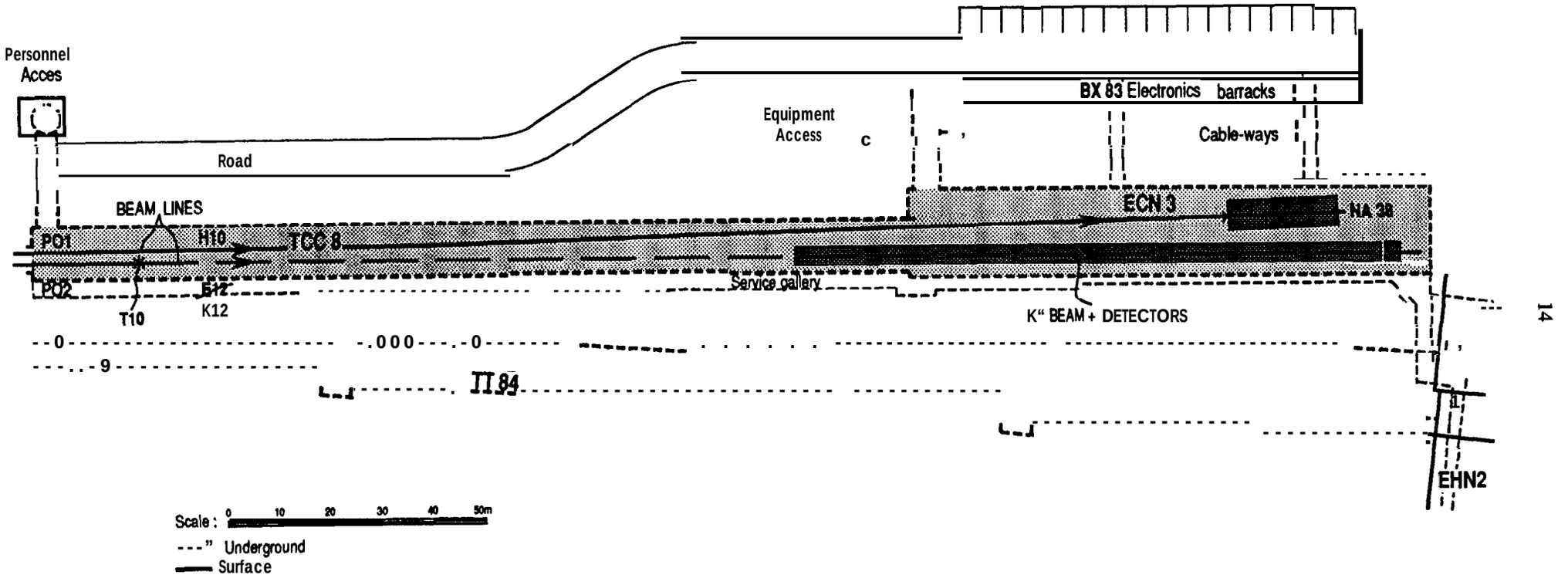

Fig, 5 Proposed layout of K^0 beam in North Area High Intensity Facility

series of S-ion runs and before the installation of the new K^0 beam and experiment. The cost of these modifications to the NA38 set-up is specified separately in Section 10.

We conclude that it seems possible to make the proposed layout compatible with a continuation of NA38, which could receive Pb-ion beams without interference, but would be in competition for proton running time.

3. TAGGING

As mentioned above, the knowledge of the origin of a decay in the K_L or K_S beam relies upon tagging of the proton producing the K_S component. This will be done by measuring the time difference between the passage of the proton in counters upstream of the K_S target (see Fig. 1) and the event time in the detector. Events with this time difference inside a given interval will be called "K_S", any other events are called "K_L". Any kind of inefficiency in the tagging counters implies that a K_S decay will be identified as a K_L decay. On the other hand, any accidental count in the counters will lead to a K_L to K_S transition. The aim is of course to keep both types of transition probability low. However, the important point is that as long as the transition probabilities are independent of the decay mode this kind of misidentifications will only lead to a dilution of the value of ε'/ε which is correctable since the dilution factor will be known with sufficient precision.

The tagging counter in the K_S beam must operate at a total rate of 10 MHz. The event time in the detector will be derived from a hodoscope in front of the electromagnetic calorimeter. The hodoscope will be preceded by a half radiation-length thick lead sheet for photon conversion. The same hardware is used to define the time for a neutral as well as for a charged decay. To diminish the effect of backsplash of photons from the electromagnetic calorimeter the hodoscope will be placed 1 m upstream of the calorimeter. To further reduce the effect of the backsplash and other accidental hits, it will consist of vertical as well as horizontal strips. Each strip will be read out from both ends and equipped with TDCs.

The time window used to identify a K_S decay has to be large compared to the time resolution of the combined tagging counter and hodoscope system in order to exclude biases from small unavoidable differences in the time resolution of charged and neutral decays. This implies that good time resolution is needed in order to limit the number of K_L to K_S transitions due to accidental protons in the K_S branch. A combined time resolution of 500 ps is expected after off-line position dependent corrections. Choosing a time window of 5 ns would then imply a 5% transition probability of K_L to K_S due to an accidental proton.

The main reason for K_S to K_L transitions will be dead time losses in the tagging counters. . . Using fast pulseheight sampling electronics read-out dead times of 2 ns can be achieved and double pulse resolutions of 5 ns[17] in each analog channel. Together with the segmentation, this will keep the dead time losses below the percent level.

The overall number of misidentifications will thus be of the order of 5%, resulting in a dilution of&'/E of 5%. This can be determined with sufficient precision by using charged decays where the vertex resolution is good enough to separate the two beams geometrically. It will also be possible to switch off one of the two beams in order to determine the dilution factors in the K_S and K_L sample.

It is of course important that there be no difference in the $K_L - K_S$ transition probabilities between charged and neutral decays. The K_L to K_S transition rate is determined by the probability of having an accidental proton in a given time interval and can thus not depend on the -decay mode of the K_L. However, as mentioned above, the K_S to K_L transitions might depend on the decay mode if the time window defining a K_S is not large enough and there is a small difference between the time resolution for charged and neutral decays. The origin of a neutral decay can be determined by using decays where one of the π^0 undergoes Dalitz decay, giving a charged vertex. The Dalitz decay thus gives a sample of neutral decays which may be used to measure the K_S to K_L transition probabilities for neutral decays. Assuming that the K_S to K_L transition probability is around 1% a sample of 10^4 Dalitz decays would measure any differences in this probability for the two decay modes to a level of 10^{-3} in the double ratio.

4. ELECTROMAGNETIC CALORIMETER

For the detection of the K^0 neutral decays, an electromagnetic calorimeter is required, with the following design performance:

a) recording of multi-photon events occurring at a rate of -1 Mhz;
b) energy resolution -3% / $E^{1/2}$ and with a constant term < 0.5%;
c) space resolution ≤ 1 mm;
d) provision of K^0 neutral event trigger with a time resolution of < 1 ns, to cope with the rate of the tagging station.

---

17 M. Atiya et al., Nucl. Instr. Methods A279 (1989) 180. An effective double pulse resolution of 8 ns has been -. achieved in spite of a relatively slow scintillator.

To satisfy these requirements the following is proposed:

i) segmentation of the detector in a transverse matrix of longitudinal cells or towers, to reduce the ambiguity in pairing of photons coming from the same π^0 and, even more important, to get higher rate capability in relationship to accidental photons;

ii) low capacitance detector channels, to allow a fast ionization charge read-out;

iii) initial current read-out technique to minimize the sampling fluctuations and to obtain short analog signals;

iv) use of liquid xenon as high density sensitive medium in a quasi-homogeneous structure, essential for applying the techniques i), ii), iii) and to satisfy simultaneously the requirements a), b), c) listed above;

v) neutral event timing trigger obtained from ionization signals.

The energy resolution achievable with a liquid xenon calorimeter has been simulated for the cell structure described below. It is shown in Fig. 6. The contribution due to electronic noise of a realistic charge read-out chain is expected to be below 30 MeV per photon. The design of the required cryostat, gas handling system and ancillary equipment is already understood in its essential elements.

The use of liquid xenon as a ionizable medium, due to its short radiation length (2.77 cm), relatively small Moliere radius (5.4 cm) and high ion-pair yield (24.3×10^3 e/mm) allows for a compact calorimeter construction with a fine tower structure subdivision. The electrode structure proposed, see Fig.7, is built from a transverse hi-dimensional array of longitudinal cells working as parallel plate ionization chambers along the beam line. Each cell is made of a central high-voltage strip surrounded at a distance of 10 mm on each side by two ground electrodes. Both high-voltage and ground electrodes are made of thin Kapton sheets, copper clad on both sides. For the signal electrodes the copper is etched in horizontal strips whose width (20 mm) defines the vertical cell structure. The Kapton foils are stretched in the vertical direction but horizontally they are bent by about 0.1 radians to the left and to the right alternately, see Fig. 7.

About 11000 towers of 2 x 2 cm^2 cross-section, each with its own read-out electronics, are needed to fill the sensitive detector volume of 2.4 m in diameter and 0.7 m in depth along the beam.

The transverse uniformity of the charge induction efficiency is ensured by the initial current read-out technique which gives a constant efficiency across the gap, except for a small region near the electrodes. With an electric field of 2 KV/cm, the total drift time T_D to cross a xenon gap is ~4 μs. With an amplifier that measures the initial current by integrating the induced charge during a time T_I = 80 ns, the response is uniform across 98% of the gap. Any residual

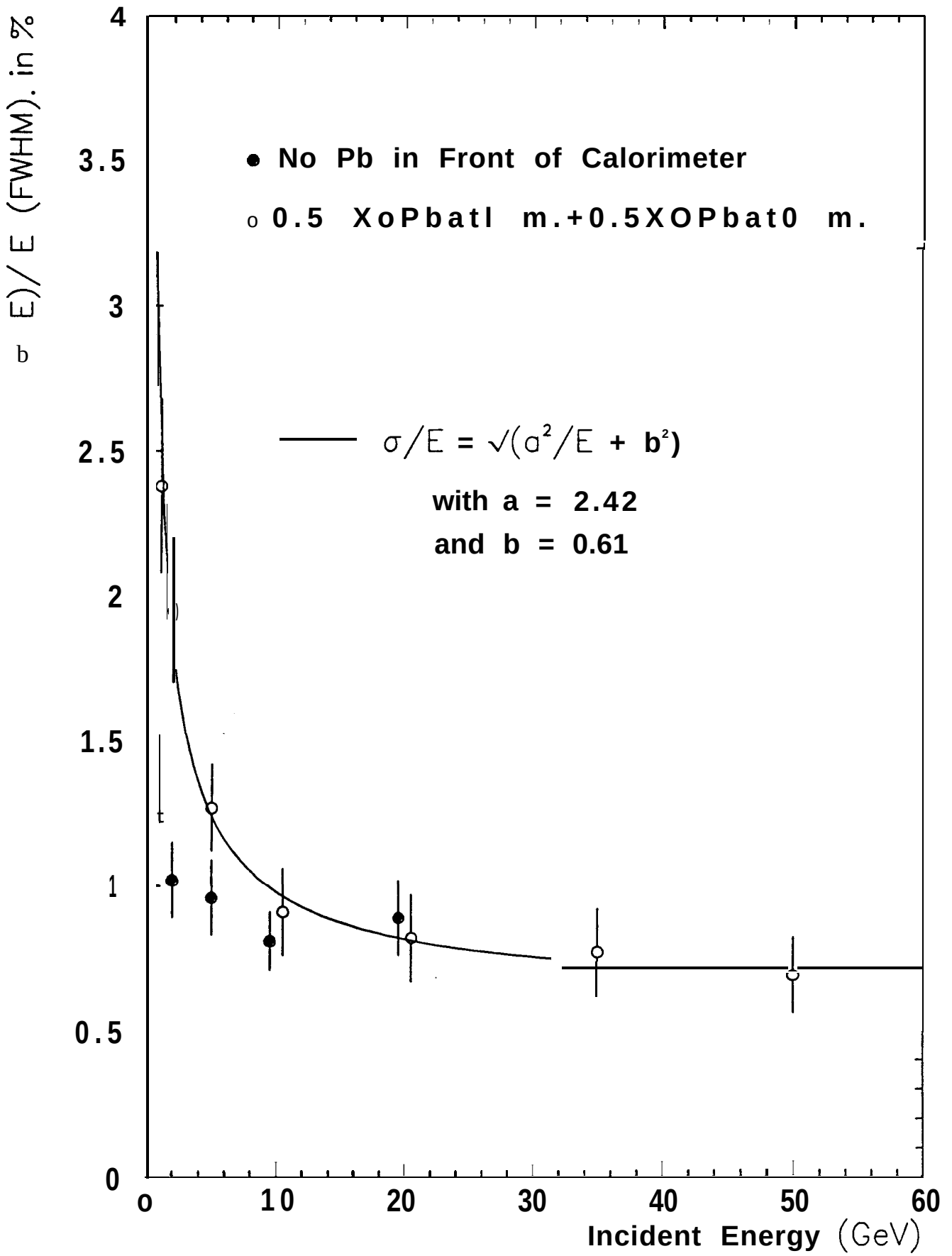

Fig. **6** Resolution of liquid xenon calorimeter

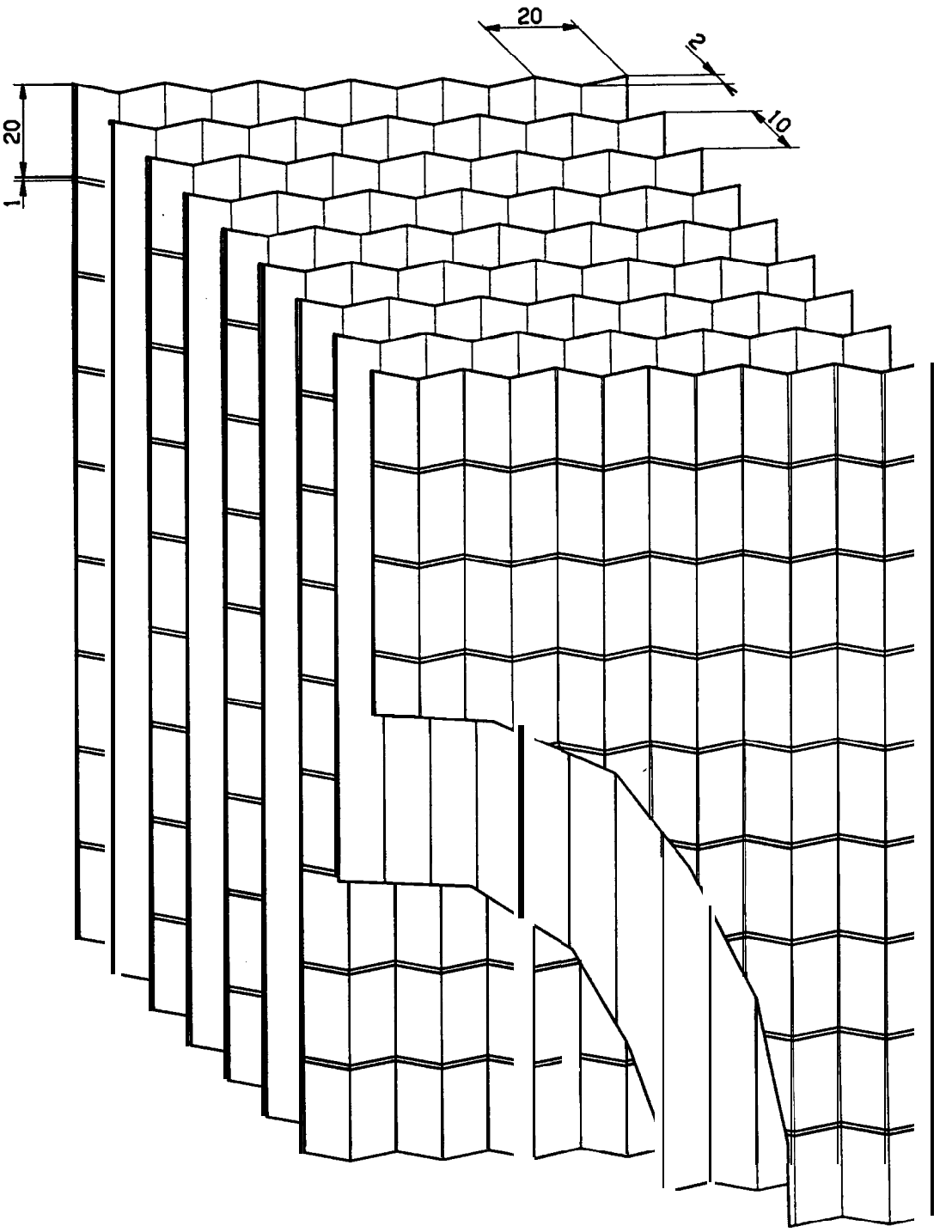

Fig. 7 Electrode structure of the liquid xenon calorimeter for particles entering from the left

gap non-uniformity as well as variations of response due to the finite thickness of the electrodes – which are never aligned with the shower axis, can be corrected off-line. It is evident that such techniques introduce an effective attenuation of the useful induced charge by a factor T_I/T_D. The induced charge signal for an em. shower with energy E is given by $Q \approx 1.2 \times 10^6$ e–. Using otherwise traditional read-out electronics the performance figures given above appear to be fully realistic.

4.1 READ-OUT ELECTRONICS

The preamplifiers are mounted directly on the read-out board, operating at liquid xenon temperature. This arrangement avoids low inductance cables which limit the speed of the charge transfer to the preamplifier[18]. Signal shaping is necessary in order to limit the band-width affecting electronic noise, and to clip the signal to 200 nsec required for triggering and fast charge read-out. A prototype analog circuit has been tested, based on a design by V. Radeka for fast liquid argon calorimetry[19].

Pulse shaping could use a conventional analog shaper followed by an analog-to-digital convertor (ADC), with a discriminator and TDC to record pulse-height and -time separately. Alternatively a flash ADC system similar to that developed for the read-out of the Aleph time projection chamber (TPC)[20] could be used, having the following features

– pulse-height read-out by interpolation, independent of precise pretrigger timing; timing to ±1 nsec per signal above -2 GeV;
– buffer memory for a number of events before final read-out.

This scheme could also be implemented as the Sigma-Delta digitizer[21], including digital pulse-shaping, if this technique becomes practical on the time scale of this experiment.

The cost of the complete read-out chain has been estimated at about 200 SFr per channel for a bilinear 2 x 8 bit dual FADC system operating at 40 MHz, based on the actual cost of the Aleph TPC read-out system. The price is expected to be similar for a conventional design based on separate function ADCS and TDCs, but is more difficult to evaluate at this stage.

---

18 V. Radeka and S. Rescia, Speed and noise limits in ionisation chamber calorimeters, Nucl. Instr. Meth. A265 (1988) 228.

19 We acknowledge the advice and co-operation of V. Radeka in procuring these circuits.

20 D. Decamp et at., Aleph: A detector for electron-positron annihilation at LEP, CERN-EP/90-25 (1990).

21 B. Hallgren and V. Hungerbühler, Possible application of the Sigma-Delta digitizer in particle physics, internal – report CERN-EP (1990).

5. MAGNETIC SPECTROMETER

The momenta of charged particles are measured in a magnetic spectrometer consisting of a central dipole magnet and two sets of drift chambers on each side (Fig. 8). With a field integral equivalent to a transverse momentum change of 200 MeV/c, the momentum resolution for one particle is limited by multiple scattering in the chamber material to $\Delta p/p = 0.6\%$. This is matched to a reconstruction accuracy of 100 μm in the chambers for the average pion momentum of 60 GeV/c if the spectrometer arms are 10 m long. The space between the chambers will be filled with helium.

A large magnet with aperture 2.45 m wide and 2.20 m high is obtained by opening the gap of an existing magnet (MNP 33), originally built with a gap of 60 cm. Additional coils will be necessary to achieve the required bending power (Fig. 9). We estimate that chambers at 2.5 m distance from the center of the magnet can operate without loss in resolution in the fringe field of the magnet, and that the nonuniformity of the field integral is less than 10%, tolerable at the trigger level.

The drift chambers are designed to have a measurement accuracy of close to 100 μm for each plane. Sufficient on-line resolution and tracking efficiency are necessary to enable a fast calculation of the decay point and the two-particle invariant mass, in order to reject decays downstream of the fiducial region and also to remove K_{e3} and $K_{\pi 3}$ decays, at the level 2 trigger, after a few μs. This can be achieved by measuring drift times with a 100 MHz clock, equivalent to 0.5 mm bins. For the off-line analysis, a further improvement of the accuracy by a factor of 4 is attainable. The average mass resolution is calculated to be 3 MeV/c^2. Accidentals and large angle δ-rays from the chamber windows can be removed by requiring a tight timing (≤ 60 ns) for the sum of the drift times in two consecutive planes, in which the sense wires are staggered (Fig. 10). The drift space of 5 mm is small enough to keep the inefficiency due to accidentals below 1%, even for the most active wires near the beam pipe. Trigger losses due to inefficiencies are avoided by doubling the measurement of horizontal coordinates. Each chamber has therefore a total of 6 sense wire planes: 4 x-planes and 2 y-planes. It is sufficient to have two planes with wires tilted by 45° (u- and v-planes) at the end of the spectrometer, in front of the calorimeter. These planes will resolve the global ambiguity which exists for most of the two-track events, and identify additional tracks scattering back from the calorimeter.

A special feature of the chambers is a central hole for the beam pipe which requires accurate construction and positioning of the ring on which the central wires end.

The rejection of K_{e3} and $K_{\pi 3}$ events at the trigger level is essential for the experiment. All events with invariant mass below 450 MeV/c^2 or transverse kaon momentum above 60 MeV/c

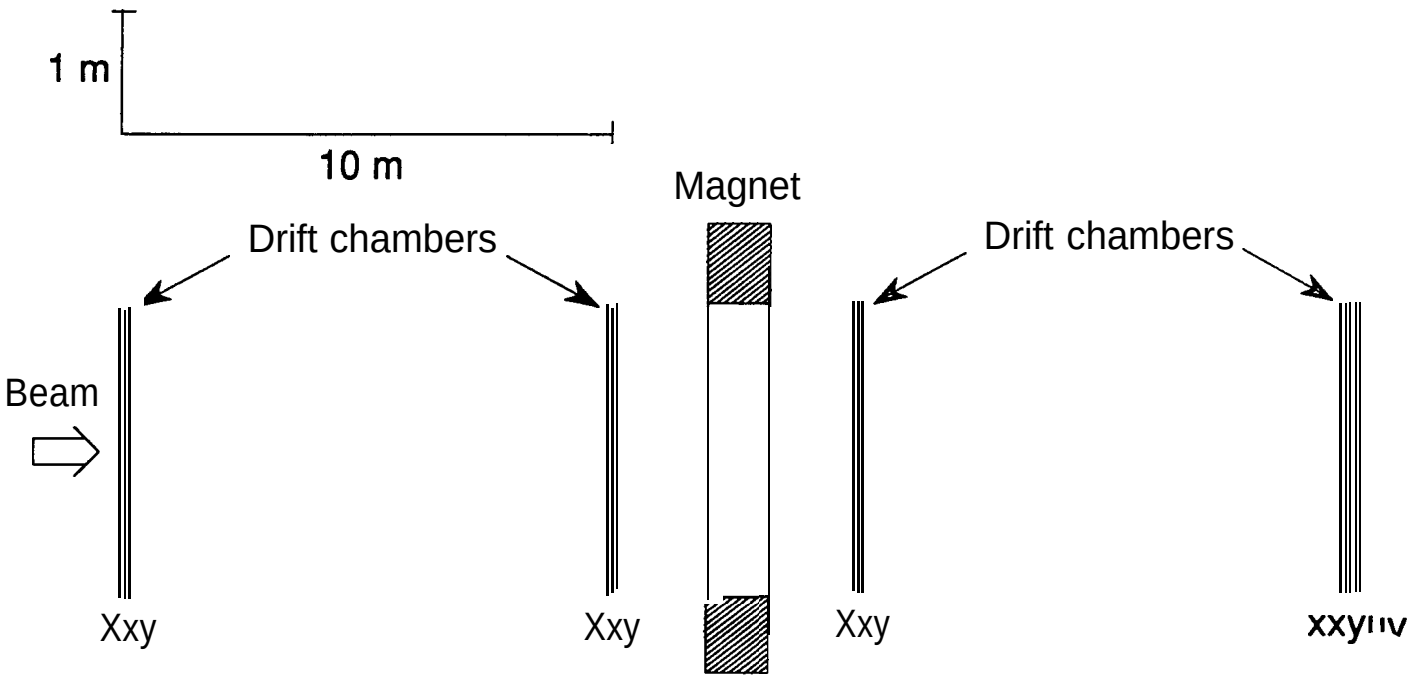

Fig. 8 Disposition of chambers and wire planes in the magnetic spectrometer

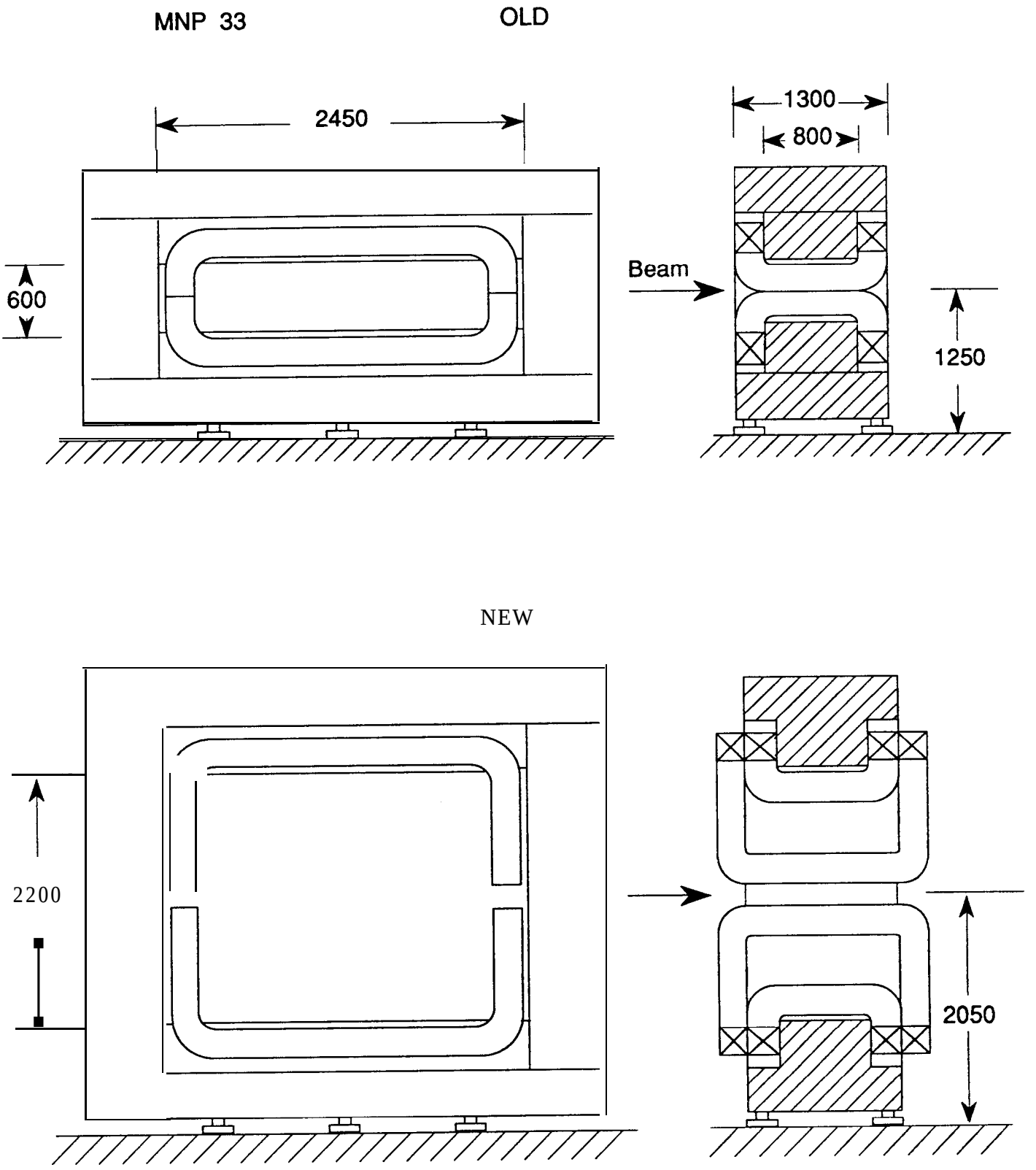

Fig. **9** Spectrometer magnet with increased gap and additional coil in the original (top) and the modified version (bottom)

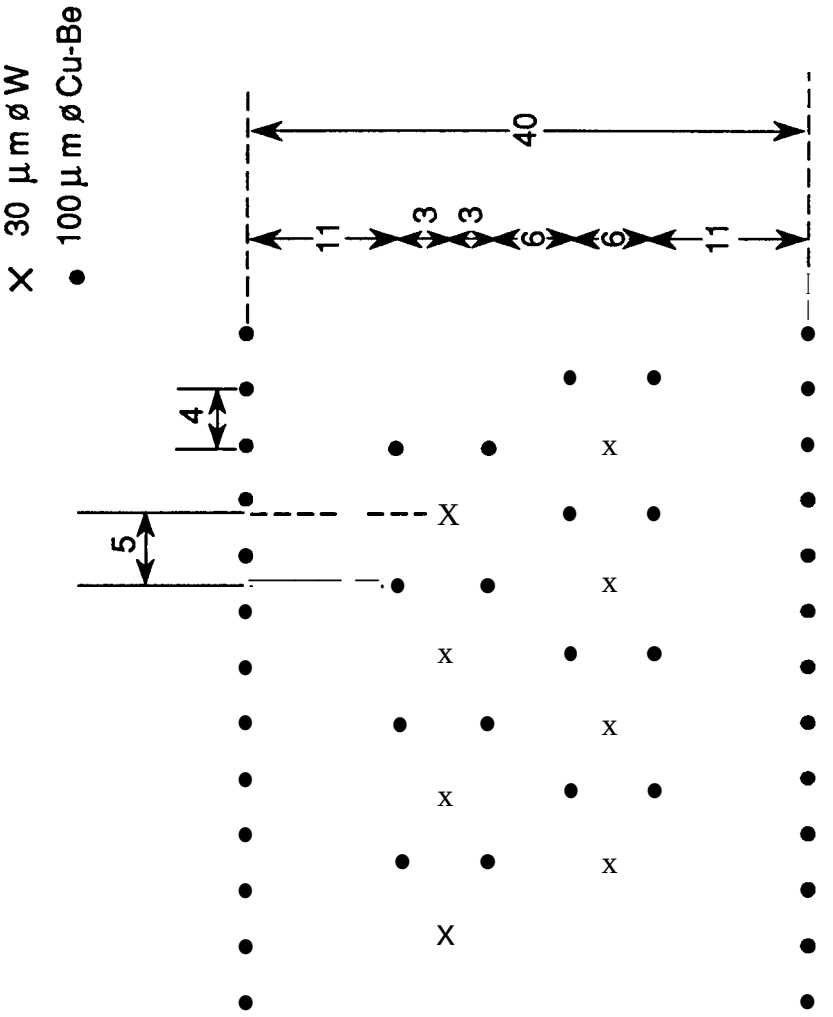

Fig. 10 Arrangement of sense wires (x), potential wires(·) and ground wires for one of the chamber planes

will be rejected. This cut removes all $K_{\pi 3}$ decays and 90% of the K_{e3} decays without loss of K $\rightarrow \pi\pi$ events. The ratio of accepted K_{e3} to $K_{\pi 2}$ events after this cut will be 20 to 1. With off-line cuts of ± 10 MeV in the invariant mass and 15 MeV/c in transverse momentum, we expect a contamination in the $K_{\pi 2}$ sample of 40% (see Fig. 11). Additional rejection of K_{e3} events by a factor of approximately 500 is obtained from the comparison of the electron energy in the calorimeter and its momentum in the spectrometer. The final contamination will then be about 1‰.

6. VETO COUNTERS

The $3\pi^0$ decay occurs at a rate 200 times that of the desired decay mode $K_L \rightarrow 2\pi^0$. It is essential to veto as much of this background in the pre-trigger as possible and thus cover a large solid angle outside the detector with ring anti-counters. These counters are arranged in eight rings at suitable longitudinal positions with angular coverage as shown in Fig. 2. The first six rings each contain two layers of 16 scintillators, each 1 cm thick, placed in pockets preceded by 5 cm and separated by 2.5 cm of iron. The last two rings are similar in structure but divided only in eight parts. Two of the existing ring pockets of the NA31 vacuum tank will be reused.

The angular acceptance of the proposed anti-counters is shown in Fig. 12. The geometrical veto efficiency for $3\pi^0$ decays is 75% at a kaon energy of 100 GeV, rising to 100% for kaons below 50 GeV.

In the charged mode it is necessary to veto the $K_{\mu 3}$ decays. For this purpose we plan to re-use the four large scintillation planes used for the NA31 muon veto. These planes will be separated from each other by about 0.8 m of iron, filling the space between the hadron calorimeter and the beam dump.

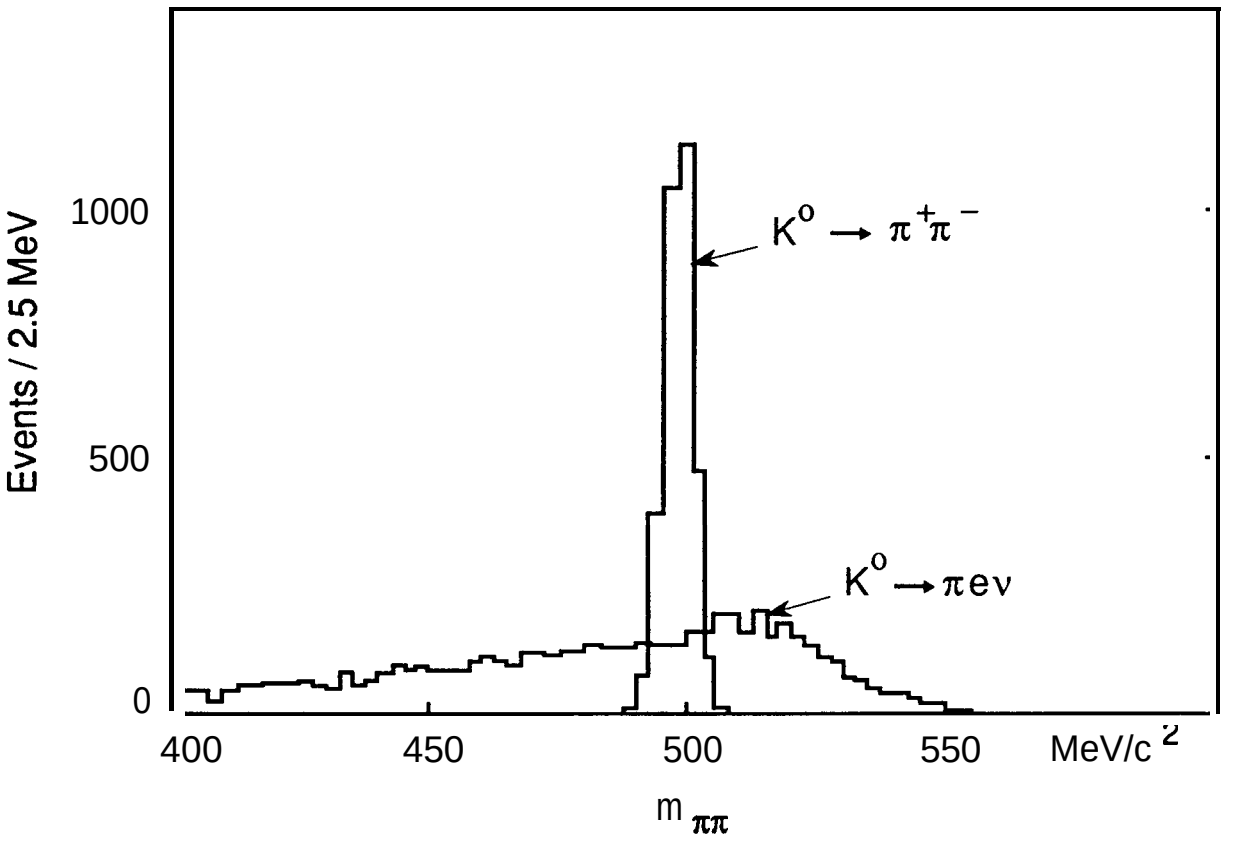

Fig. 11 Invariant mass of $K_{\pi 2}$ and K_{e3} events with $p_\perp < 15$ MeV/c

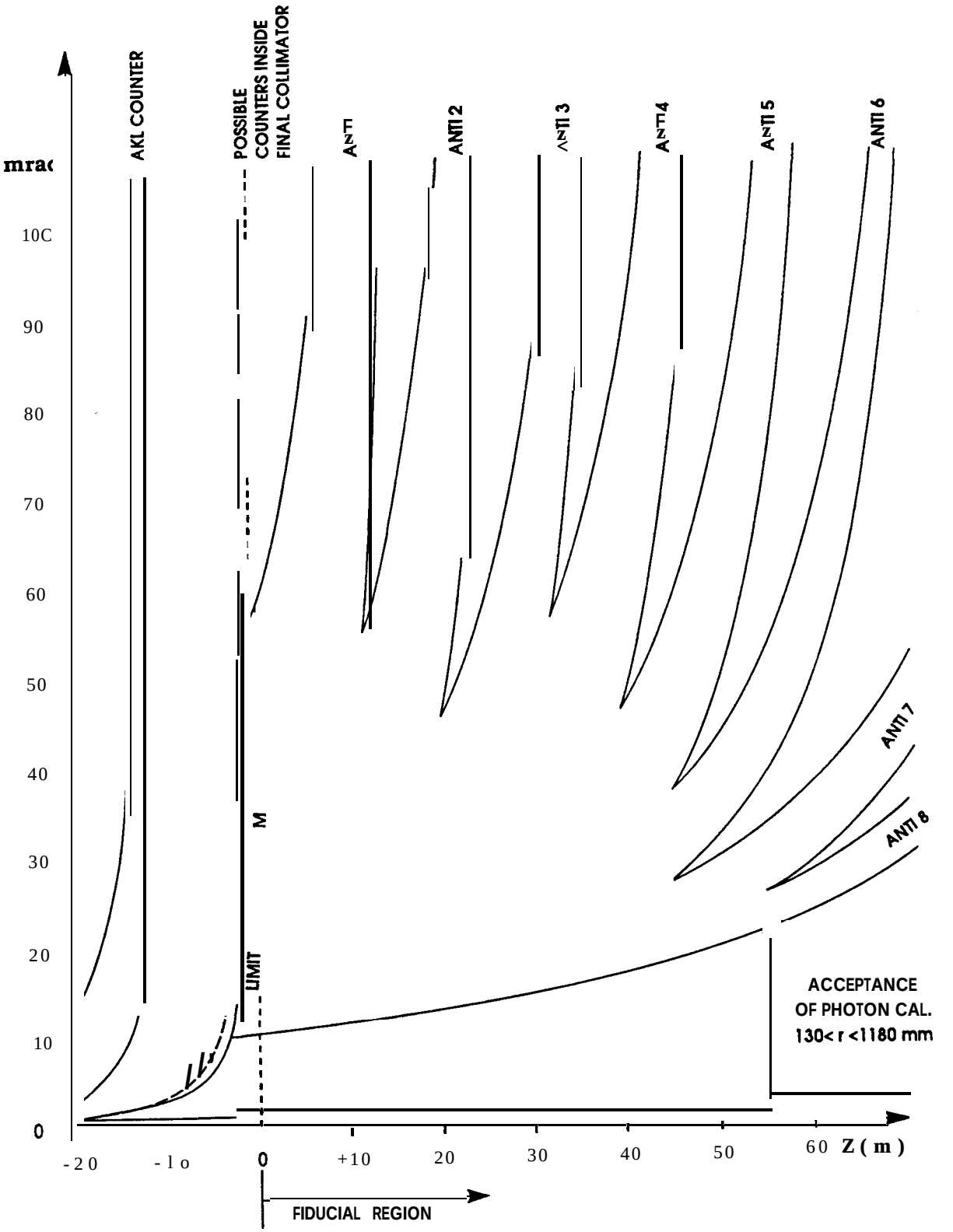

Fig. 12 Angular acceptance of anticounters

7. TRIGGER

The design criteria for the trigger assume that the beam rates will be about twenty times that of the NA31 experiment. High rate handling capability, large and unbiased background rejection and minimal deadtime can only be achieved with a multi-stage trigger. Therefore the trigger design consists of three stages of increasing complexity. The expected rates at all three levels have been estimated by Monte Carlo and are summarized in Table 2.

Table 2: Trigger rates per second

Mode	$\pi^+\pi^-$	K_{e3}	$K_{\mu 3}$	$\pi^+\pi^-\pi^0$	$2\pi^0$	$3\pi^0$	Total
Branching ratio	0.0020	0.39	0.27	0.12	0.0009	0.22	1
Total K_L Decays with 20 GeV/c < p < 200 GeV/c and –10 m < z < 100 m	612	116k	81k	37k	273	65k	300k
Level 1	212	20k	7k	7k	104	12k	46k
Level 2	37	0.7k	0.1k	–	10	0.5k	1.5k

Level O Pretrigger – using trigger hodoscope information. The pretrigger provides the timing for the subsequent stages of the trigger. Its total rate is expected to be less than 1 MHz, out of which about 300 KHz come from K^0 decays. The signal will be available after about 100 ns. For charged decays, it will be the coincidence of hits in the trigger hodoscope on opposite sides of the beam pipe. For neutral decays, a single hit in the trigger hodoscope in coincidence with a fast energy sum signal from the calorimeter will be required.

Level 1 Fast two particle trigger – using muon veto, photon anticounter and energy threshold information in coincidence with the driftchamber and hadronic calorimeter signals for charged events and cluster information in the electromagnetic calorimeter for neutral events. It is planned tore-use the NA 31 hadron calorimeter, placed immediately after the electromagnetic calorimeter. It will be used only to give energy thresholds and be part of the muon veto. The rate after Level 1 will be less than 100 KHz, of which about 20% will be purely neutral. The signal will be available after about 500 ns.

Level 2 Fast event reconstruction in hardware – using $p_\perp$ balance, vertex, energy and mass cuts for charged events and centre of gravity, vertex and refined energy cuts for neutral events. The output rate will be less than 2 KHz. The signal will be available about 9 μsec later.

Level 3 Full event reconstruction in special processors by software. This will be integrated with the data acquisition system.

The elements of the neutral trigger scheme are well defined. In order to reduce the substantial $3\pi^0$ rate at the first level, cuts will be applied on the number of electromagnetic clusters found in the horizontal and vertical projections of the electromagnetic calorimeter, together with a threshold on the electromagnetic energy. The number of charged triggers which also satisfy the neutral trigger conditions will be reduced by requiring that there be very little energy in the hadron calorimeter.

The principal cuts at the second level are on the total energy, the centre of gravity of the energy deposition in the electromagnetic calorimeter, and on the reconstructed vertex of the presumed $2\pi^0$ decay. The small beam size, short fiducial region and excellent calorimeter resolution will allow tight cuts to be applied. The $3\pi^0$ background will be greatly reduced at the second level by a simple vertex cut calculated from the second moments of the energy distribution; such events have missing high energy photons which displace the apparent vertex calculated assuming the $K \rightarrow 2\pi^0$ hypothesis toward the detector by typically 20 m. It may be possible to reduce still further the remaining $3\pi^0$ background by identifying the number of photons at the second level.

Table 3: Principal trigger conditions

Trigger conditions		
Level	Charged trigger	Neutral triggers
1	2 hits in trigger hodoscope (opposite quadrants) >35 GeV total energy 2 or more hits in all D.C.'s	1 hit in trigger hodoscope >40 GeV electromagnetic energy <5 peaks in each calorimeter projection
2	Total energy between 40 and 200 GeV Decay between -2 and 5 K_S lifetimes from collimator Transverse momentum <60 MeV/c, centre of gravity < 15 cm	

The main charged trigger rate after the frost level arises from K_{e3} and, to a lesser extent from $K_{\mu 3}$ and $\pi^+\pi^-\pi^0$ decays; most of the $K_{\mu 3}$ decays are vetoed by the muon hodoscope, and those that remain arise mainly from events in which the muon either misses the hodoscope, or is absorbed in the iron before reaching the last plane of the muon veto system. Some rejection of the three body decays is achieved at the first level by requiring hits on opposite sides of the beam pipe, and can be augmented by conditions on the number of hits in the drift chambers which are required to be consistent with two charged particles. Low energy decays, and some K_{e3} rejection, is obtained by requiring that energy be deposited in the hadron calorimeter.

The most effective rejection criterion for the charged decays is the K^0 mass – all the $\pi^+\pi^-\pi^0$ decays have a 2π mass less than 0.36 GeV/c^2, and are thus easily removed. Of the&3 which survive, only 10% have a $\pi\pi$ mass between 0.45 and 0.55 GeV/c^2; most of the remaining $K_{\mu 3}$ decays are also rejected by this cut. In order to ensure that the biases on the 2π decays are kept small, this cut should be effectively greater than four standard deviations, which implies that the on-line mass resolution be smaller than about 12 MeV/c^2. The main problem with fast calculation of the effective mass concerns the "tracking" through the magnetic field. It is proposed to use look-up tables both to find the tracks and to compute the momenta. This imposes limits on the number of bits/point allowed. Simulations show that, with 8-bits for each chamber displacement measurement, it is possible to reconstruct the K^0 mass to better than 10 MeV/c^2 precision, provided that the chamber resolution on-line is better than 0.5 mm. The field mapping can be coarse grained since the field integral is expected to vary by less than 10% over all relevant paths. In addition, cuts can also be applied on the total energy, vertex position and missing transverse momentum. The track finding, mass, vertex, energy and $p_\perp$ reconstruction in special purpose hardware will take about 10 p-seconds. This reduces the rate sufficient y to allow conventional processors to perform full event reconstruction, for rejection of most of the remaining K_{e3} and $3\pi^0$ background, incomplete decays etc. The rate at this level is determined by the number of calibration and monitoring events required

8. DATA ACQUISITION

The experiment could produce up to 10^4 events per second with a size of 4 Kbytes, giving a data rate of 40 Mbytes per second or 100 Mbytes per burst. To handle this we propose an acquisition system consisting of 10 transputers (or equivalent) connected to a common bus with a transfer capacit y of 100 Mbytes/sec. Including system arbitration, the transfer of an event to one of the transputers will take less than 50 μsec. Simple calculations and data storing will need an additional 450 μsec, so that a 10 transputer system can sustain an input rate of 2 x 104 events/second. Each transputer board needs a 16 Mbyte memory to buffer the data from one burst, which could be expanded to 32 Mbytes if necessary. Further analysis of the data stored _

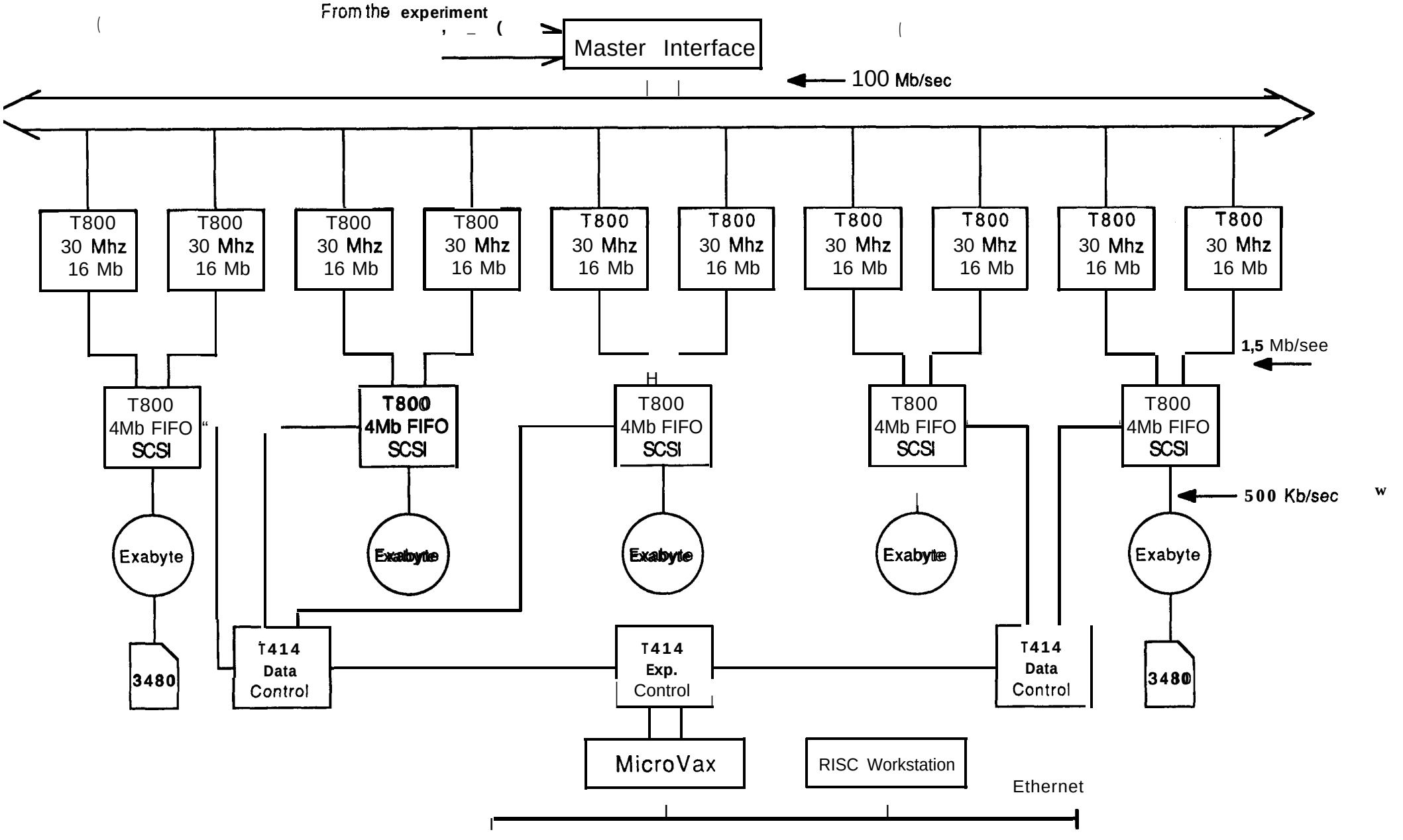

Fig. 13 Data acquisition read-out scheme

during the burst will be done in the 12 seconds between bursts, thus giving 5 msec of computing time per event.

For a filter rejection factor of three the output rate from each CPU will be less than 250 Kbytes/see, matching the transfer speed of Exabyte tape drives with an SCSI interface. New tape drives are amounted with 500 Kbytes/sec interfaces, allowing one such drive to be shared between two CPUs. With a better rejection factor at the trigger level, the input rate will be correspondingly lower, and the CPUS could do a full reconstruction of each event.

An implementation of this readout scheme is shown in Fig. 13. Everything is available on the market except for a suitable master interface which copies the events from the experiment to the transputer memories. Filtered events are transferred at 1.5 Mbytes/see via the serial transputer link to a transputer which has an SCSI interface to the Exabyte drive. Other transputers handle the control of the system and the interface to the host machine for programme downloading, network access, user interaction, etc. The system can handle up to 100 Mbytes per burst of data with a rejection factor of three, or 36 Mbytes per burst with no rejection.

8.1 RECONSTRUCTION

The reconstruction procedure needs some consideration. The CERN Computing Centre does not yet support Video 8 tapes, although a central Exabyte <-> 3480 copying facility will be established. The transputer system described above can be used as a private reconstruction or Monte Carlo computing facility with 10 CPUS plus a fraction of the tape drivers CPU usable in background. Assuming better compilers and faster transputers will give 1.5 IBM 168 units for each CPU, we may have 18 units available 24 hours a day. A powerful RISC station (Decstation 5000 or IBM 6000) can be added as another front-end computer with powerful graphics and additional CPU power; for example, to do the reconstruction during data taking. The system is in itself an Exabyte copying station, and by adding 3480 drives to a pair of T800 one could also have an Exabyte to 3480 copying station.

9. SUMMARY

The proposed experiment is designed to operate in an instantaneous single particle flux of 10^6 Hz requiring a beam intensity of 1.5 x 10^{12} protons per pulse on target. Under these conditions 1.5 x 10^6 useful $K_L \rightarrow 2\pi^0$ decays are accumulated in one year of data-taking, of effectively 120 days at 50% overall efficiency. Two to three years of operation with at least 120 days each

are required for a result with 1 x 10^{-3} statistical uncertainty on a measurement of the double ratio R of K_S and K_L decay rates into $2\pi^0$ and $\pi^+\pi^-$, respectively.

The dominant systematic uncertainties are expected to arise from possible differences in the reconstructed energy scales of $K^0 \rightarrow 2\pi^0$ and $K^0 \rightarrow \pi^+\pi^-$ decays, and from the residual three body decay backgrounds to the CP violating two-body decay modes. A relative energy scale error of 1 in 1000 seems achievable, and would result in a 1 per mille uncertain yin the double ratio. Backgrounds should be at a level of 0.2% to 0.3%, or below, and would contribute each ~0.3 per mille uncertainty. The total systematic uncertainty on the double ratio is expected to be around 1 per mine. With statistical and systematic errors combined an uncertainty of 2 x 10^{-4} on Re ε'/ε can therefore be expected.

Construction of the necessary equipment requires three years, depending strongly on the funding rate. Initial installation and component testing are planned for 1993, while data taking might start in 1994, lasting until 1996 and requiring at least 120 days of SPS fixed target operation per calendar year.

10. COST

A breakdown of the cost for new equipment is estimated as follows (in KSFr), listed according to the Section numbers used in the foregoing description.:

2. Beam

K_L beam	**360**
K_S beam	**230**
Vacuum tank and window	**320**
Instrumentation and controls	100
Magnet power and cooling	130
Assembly and installation	360
	1500

3. Tagging system

Scintillators, photomultipliers and electronics	400
	400

4. Electromagnetic calorimeter

Cryostat	800	
Window	100	
Read-out boards	400	
Xenon buffer and purification	1500	
		2800

Electronics (12 000 channels)

Preamplifiers	300	
Cables	100	
Pulse shaping	300	
Digitizers	900	
Read-out and crates	700	
Calibration system	100	
		2400

5. Magnetic spectrometer

Magnet modifications	200	
Drift chamber mechanics	1000	
Read-out electronics	1100	
Cables	100	
Helium enclosure	200	
Gas system	100	
		2700

6. Veto system

Scintillators, phototubes and cables	750	
Six anticounter ring pockets	150	
		900

7. Trigger system

Levels O and 1	500	
Level 2 neutral	500	
Level 2 charged	500	
		1500

8. Data acquisition

Transputer system with Fastbus interface	300	
5 Exabyte drives with crates etc.	60	
Microvax 3200	80	
2 cassette tape drives with interface	60	
Workstation	150	
		650
TOTAL		**12900**

Modifications to NA38 structures are estimated at 390 kSFr. The costs of installing, filling and operating the detector have not been included in this estimate.

APPENDIX

Study of CP violation asymmetries in $K^{\pm} \to 3\pi$ decays

In addition to causing a difference between $|\eta_{00}|^2$ and $|\eta_{+-}|^2$, direct CP violation is expected to produce an asymmetry *in* the C.M. energy distribution for pions of opposite charge from $K^{\pm} \to 3\pi$ decay.

For example, in a recent paper Bel'kov et al.[22] on the basis of the value of $\varepsilon'/\varepsilon = 3.3 \times 10^{-3}$ as measured byNA31, calculate:

$$Ag = 1.4 \times 10^{-3}$$

where $Ag = (g^+ - g^-)/(g^+ + g^-)$ with g+, g- defined as the slope as a function of x of the density of decays in the Dalitz plot and

$$x = \frac{2M_k}{m_\pi^2}\left(\frac{M_k}{3} - W^{\pm}\right),$$

where $W^{\pm}$ is the C.M. energy of the pion with charge opposite to the charge of the decaying kaon.

With appropriate substitution of the front end of the beam by an achromatic charged particle transport system, it appears possible to have entering the normal decay region, in place of the neutral beams, a beam consisting at the same time of both positive and negative particles, roughly analyzed in momentum with the same size and divergence as the neutral K beam.

Without any need for changes to the hardware of the experimental set up, the 37c decays from K^+ and K^- can be identified and accurately measured. Data could be taken with alternating polarity for the magnetic field of the spectrometer and the distributions in x obtained for both $\pi^-\pi^+\pi^+$, $\pi^+\pi^-\pi^-$ and $\pi^{\pm}\pi^0\pi^0$ from $K^{\pm}$ decays in a situation where to a very good accuracy the acceptance of the detection system, including the effect of accidentals, would be automatically the same for the $\pi^{\pm}$ because of the space-time overlap of the K^+ and K- (and accompanying particles) in the beam seen by the detector.

This principle holds the promise for drastically improving the systematic accuracy with respect to previous experiments and the intensity achievable for the beam coupled with an adequate data acquisition system will allow a large increase in statistics.

---

22 A.A. Bel'kov et al., Prediction of direct CP violation for $K \to 3\pi$ decays in chiral perturbation theory, Phys. Len. 232B (1989) 118.

A simple Monte Carlo simulation shows that in a one year running period with 3 x 10^5 effective SPS pulses, a total of 2 x 10^8 $K^{\pm}$ –> 3π decays could be collected with a resulting accuracy of 3σ (an improvement by more than one order of magnitude with respect to the present experimental situations) for the Ag = 1.4 x 10^{-3} effect quoted above.

The importance of being able to detect with the same experimental setup direct CP-violation effects in charged kaon decays as well as by comparing $|\eta_{00}|^2$ with $|\eta_{+-}|^2$ cannot be overemphasized.

Imprimé au CERN. Prix : 1.50 Fr.